ICES Journal of Marine Science

ICES Journal of Marine Science (2018), 75(7), 2355–2369. doi:10.1093/icesjms/fsy088

Contribution to the Symposium: '*Ecosystem Studies of Subarctic and Arctic Seas*'

Original Article

Future ecosystem changes in the Northeast Atlantic: a comparison between a global and a regional model system

Morten D. Skogen[1,2,*], Solfrid S. Hjøllo[1,2], Anne Britt Sandø[1,2], and Jerry Tjiputra[3]

[1]*Institute of Marine Research, Bergen, Norway*
[2]*Bjerknes Centre for Climate Research, Bergen, Norway*
[3]*Uni Research Climate, Bjerknes Centre for Climate Research, Bergen, Norway*

**Corresponding author: tel: +47-91712689; e-mail: morten@imr.no.*

Skogen, M. D., Hjøllo, S. S., Sandø, A. B., and Tjiputra, J. Future ecosystem changes in the Northeast Atlantic: a comparison between a global and a regional model system. – ICES Journal of Marine Science, 75: 2355–2369.

Received 10 November 2017; revised 14 June 2018; accepted 18 June 2018; advance access publication 19 July 2018.

The biogeochemistry from a global climate model (Norwegian Earth System Model) has been compared with results from a regional model (NORWECOM.E2E), where the regional model is forced by downscaled physics from the global model. The study should both be regarded as a direct comparison between a regional and its driving global model to investigate at what extent a global climate model can be used for regional studies, and a study of the future climate change in the Nordic and Barents Seas. The study concludes that the global and regional model compare well on trends, but many details are lost when a coarse resolution global model is used to assess climate impact on regional scale. The main difference between the two models is the timing of the spring bloom, and a non-exhaustive nutrient consumption in the global model in summer. The global model has a cold (in summer) and saline bias compared with climatology. This is both due to poorly resolved physical processes and oversimplified ecosystem parameterization. Through the downscaling the regional model is to some extent able to alleviate the bias in the physical fields, and the timing of the spring bloom is close to observations. The summer nutrient minimum is one month early. There is no trend in future primary production in any of the models, and the trends in modelled pH and Ω_A, are also the same in both models. The largest discrepancy in the future projection is in the development of the CO_2 uptake, where the regional suggests a slightly reduced uptake in the future.

Keywords: Barents Sea, climate change impacts, downscaling, Greenland Sea, Norwegian Sea

Introduction

Human influence on the climate system is clear, and recent climate changes have had widespread impacts on human and natural systems. Without action, the world's mean surface temperature is projected to rise over the 21st century (IPCC, 2014). Global coupled climate models (GCM) are generally capable of reproducing the observed trends in, e.g. the globally averaged atmospheric temperature. However, the global models do not have the horizontal resolution, which is needed in order to properly resolve the relevant features on regional scales (Melsom *et al.*, 2009). As the spatial scales represented by the GCM may not be as fine as the end-use application requires, the GCM outputs will contain biases relative to the observational data, which preclude its direct use. Therefore, dynamical downscaling using so-called Regional Climate Models (RCM) is necessary to translate coarse global scale information into fine regional and local grids in order to obtain climate information on scales that are relevant to society.

Over the past years, the emerging impacts of climate change on the Northeast Atlantic ecosystem have caused serious concerns (e.g. Fossheim *et al.*, 2015; Eriksen *et al.*, 2015). In the Polar regions, and in particular in the Arctic, there is significant spatial variability among GCMs (Overland and Wang, 2007; Steinacher *et al.*, 2009). The Arctic region will continue to warm more

rapidly than the global mean, and this, together with the systems limited adaptive capacity, makes the Arctic more vulnerable to climate change (IPCC, 2014). Therefore, any attempt to evaluate future ecosystem consequences of CO_2 emissions will need predictions of ocean biogeochemistry changes at regional scale, along with detailed knowledge of biological responses. Some previous studies have focused on regional biogeochemistry in the Atlantic section of the Arctic Ocean. Using downscaled regional ocean models Bellerby *et al.* (2012) modelled both present and future climate ocean acidification in the Arctic with a focus on the Spitsbergen region, and Skogen *et al.* (2014) did a similar study of changes in ocean acidification for the whole Barents and Nordic seas. Skaret *et al.* (2014) and Slagstad *et al.* (2015) on the other hand, focused on changes in primary and secondary production in their studies with focus on the Barents Sea and the Arctic Ocean, respectively.

For proper interpretation of climate change projections from RCMs, it is important to first assess the signal of climate change from GCMs to RCMs. This has been done for the atmosphere in a number of publications (e.g. Saini *et al.*, 2015). Langehaug *et al.* (2018) used a high 0.25° and a medium 1.0° version of the global ocean-sea ice component of the Norwegian Earth System Model (NorESM1-ME) to assess the impact of increased ocean resolution, but to our knowledge there has not been any comparison of results from a GCM and a RCM. The goal of the present paper is to quantify whether an ocean RCM produce different projections than its driving GCM, based on climate change projections for the Nordic and Barents Seas. The performance and projected changes of the RCM are examined and compared with those of the driving GCM, thus the present study should be regarded as both a direct comparison between an RCM and its GCM and a study of the impact of climate change scenarios in the area. To achieve this a GCM (NorESM1-ME) has been downscaled and used to force a biogeochemical RCM (NORWECOM.E2E) for the Barents and Nordic seas under the RCP4.5 emission scenario. The focus has been on comparing model outputs on ocean carbon chemistry and primary production to investigate how the global and regional model compare for some key parameters. Such a comparison could provide new insights both on how well a GCM projection changes on a regional scale, and which future ecosystem questions can sufficiently be answered by a GCM with enough confidence.

Material and methods

NorESM1-ME

The NorESM1-ME is a fully coupled climate carbon cycle model developed in Norway in collaboration with researchers from the National Center for Atmospheric Research at the United States. As such, some of its components are adopted from the Community Climate System Model (CCSM4), i.e. the atmospheric general circulation (Community Atmospheric Model, CAM4), land (Community Land Model, CLM4), and sea-ice (Community, CICE4) components (Gent *et al.*, 2011). The ocean physical circulation is based on the Miami Isopycnic Coordinate Ocean Model (MICOM), coupled with the Hamburg Oceanic Carbon Cycle (HAMOCC5) model (Maier-Reimer *et al.*, 2005; Tjiputra *et al.*, 2013).

In the upper ocean, the HAMOCC5 model consists of an NPZD-type ecosystem module, where the primary production is formulated as a function of phytoplankton growth and nutrient concentration within the top 100 m. In addition to multi-nutrients (i.e. nitrate, phosphate, and dissolved iron) co-limitation, the phytoplankton growth is limited by light availability and temperature. Simpler than the NORWECOM.E2E, HAMOCC5 model simulates a generic single class phytoplankton and zooplankton compartments. Below the mixed layer, particulate materials (particulate organic carbon, biogenic opal and calcium carbonate) sink at constant velocities and are remineralized at depth. Silicate (SI) concentration does not limit phytoplankton growth but is used to determine the portion of biogenic opal and calcium carbonate export production. Non-remineralized particles reaching the bottom layer, undergo chemical reactions with sediment porewaters, bioturbation and vertical advection within the sediment module.

The formulations of the ecosystem dynamics are described in Six and Maier-Reimer (1996) and Maier-Reimer *et al.* (2005). In contrast to the NORWECOM.E2E, the ecosystem parameters in NorESM1-ME (HAMOCC5) are tuned toward the global marine ecosystem. The parameters in the HAMOCC5 model are tuned to optimize the large scale spatial distribution of surface primary production and biogeochemical tracers in the interior in order to reproduce the observed climatology features as well as the global ocean carbon sources and sinks. More details of the evaluation and performance of the ocean biogeochemistry in the NorESM1-ME model is available in Tjiputra *et al.* (2013). In this study, we apply the standard coupled RCP4.5 projection, following the standard CMIP5 (Coupled Model Intercomparison Project phase 5) protocol (Taylor *et al.*, 2012). The RCP4.5 represents a future scenario where the global mean atmospheric radiative forcing approach 4.5 W m^{-2} by year 2100. Under this scenario, the atmospheric CO_2 concentration pathway reaches 538 ppm at 2100. For the comparison with the regional model, we focus on analysing results from the 2006 to 2070 periods.

ROMS downscaling

To downscale the NorESM1-ME model (producing the physical forcing for the regional biogeochemical model), the Regional Ocean Modeling System (ROMS, Shchepetkin and McWilliams, 2005) is used. The ROMS model set-up is initialized from the NorESM1-ME model, and outputs from NorESM1-ME are also used at the open boundaries and as atmospheric forcing. A weak relaxation towards NorESM1-ME sea surface salinity with a time scale of 360 days was also applied. The model domain for the ROMS downscaling covers the North Atlantic, the Nordic and Barents Seas, and the Arctic Ocean from 30°N to the Bering Strait, with a horizontal model resolution of $\sim 10 \times 10$ km. In the vertical 35 generalized σ-coordinate (s) levels, stretched to increase vertical resolution near the surface and bottom, were used. The time step was 100 s. The ROMS model on this grid has previously been evaluated in a hindcast study in Melsom *et al.* (2009) and Sandø *et al.* (2014). Here, it was shown that downscaling reduced the biases in the Barents Sea projected by the global model, and that the downscaled results generally were closer to observations. For the present study the regional ROMS model was run for the period 2006–2070. More details on the set-up and performance of the present downscaling can be found in Sandø *et al.* (2018).

NORWECOM.E2E

The NORWegian ECOlogical Model system End-To-End (NORWECOM.E2E), a coupled physical, chemical, biological model system (Aksnes *et al.*, 1995; Skogen *et al.*, 1995; Skogen and

Søiland, 1998), was developed to study primary production, nutrient budgets and dispersion of particles such as fish larvae and pollution. The model has been validated by comparison with field data in the Nordic and Barents seas (Skogen *et al.*, 2007; Hjøllo *et al.*, 2012; Skaret *et al.*, 2014). Recently, it has been extended with a module to project ocean acidification (Skogen *et al.*, 2014), and with Individual Based Models (IBMs) for *Calanus finmarchicus* (Hjøllo *et al.*, 2012) and pelagic fish (Utne *et al.*, 2012).

In the present study, the model is run in offline mode. Physical ocean fields (velocities, salinity, temperature, water level and sea ice) from the ROMS downscaling (Section 2.2) has been interpolated from 5-daily means and used as physical forcing together with daily atmospheric (wind and short wave radiation) fields from the NorESM1-ME (Section 2.1) simulation. The horizontal grid used (Figure 1) is identical to a subdomain of the original ROMS grid, while in the vertical 20 sigma layers are used. The time step is 3600 s.

The biochemical model is coupled to the physical model through the light, the hydrography and the horizontal and vertical movements of the water masses. The prognostic variables are dissolved inorganic nitrogen (DIN), phosphorous (PHO), and SI, two different types of phytoplankton (diatoms and flagellates), two detritus (dead organic matter) pools (N and P), diatom skeletal (biogenic silica) and oxygen. Two types of zooplankton (meso- and micro-zooplankton) are included based on a module taken from the ECOHAM4 model (Moll and Stegert, 2007; Stegert *et al.*, 2009; Pätsch *et al.*, 2009). The processes included are primary and secondary production, grazing by zooplankton on phytoplankton and detritus, respiration, algae death, remineralization of inorganic nutrients from dead organic matter, self shading, turbidity, sedimentation, resuspension, sedimental burial, and denitrification. The material produced by mortality is partly regenerated through the detritus pool, but a fraction of 10% is instantly regenerated as DIN (in nature as ammonia) and 25% as PHO available for uptake by phytoplankton (Garber, 1984; Bode *et al.*, 2004).

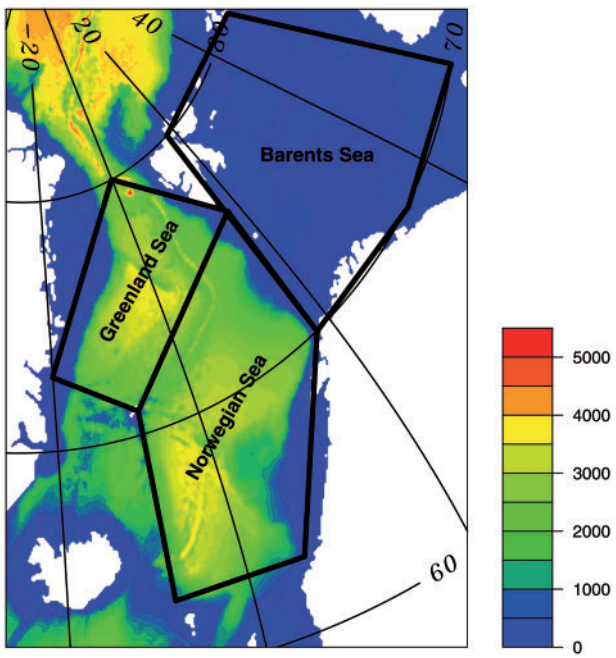

Figure 1. Model domain for NORWECOM.E2E with bathymetry and boxes indicating the three seas used for statistics (Barents Sea, Greenland Sea, and Norwegian Sea). Shading denote water depth in meters.

Ocean acidification is modelled using a submodule (Blackford and Gilbert, 2007; Skogen *et al.*, 2014) for the carbonate system. The module is an implementation of the Haltafall speciation code (Ingri *et al.*, 1967). The module calculates the carbonate system at any given point in space and time, using constants from Mehrbach *et al.* (1973) refitted by Dickson and Millero (1987). The inputs are temperature, salinity, dissolved inorganic carbon (DIC), total alkalinity (TA), and depth (pressure), whereas the outputs are pH, partial pressure of CO_2 in seawater, carbonate and bicarbonate ion concentrations, and calcite and aragonite calcification states. In addition, the module calculates the air sea exchange of CO_2 taking into account wind speed and atmospheric pCO_2. The latter one uses the (Nightingale *et al.*, 2000) parameterization for gas transfer velocity. TA is not a prognostic variable in the model. For oceanic regimes there is generally a well constrained relationship between salinity and TA as TA is conservative, and in the model an expression for the Nordic Seas and North Atlantic from Bellerby *et al.* (2005) ($TA = 66.96 \times S - 36.803$) have been used for the calculation of TA. To allow the integration of the carbon system three state variables are added [detritus C pool, dissolved organic carbon (DOC) and DIC]. The carbon fluxes are following the nitrogen fluxes using the Redfield ratio [C:N = 5.68 (weight)], except for the remineralization rate of detritus C to DOC (10% day^{-1}) taken from ECOHAM4 and the degradation rate of DOC (6% day^{-1} at 8 degrees, and Q10 = 2.6), which is taken from Lønborg *et al.* (2009). The new state variables have no impact on parameters in the original biogeochemical model. Future scenario of the atmospheric CO_2 concentration based on the RCP4.5 of the fifth assessment report of the IPCC (2013) (Table AII.4.1), is used for the atmospheric boundary condition. Remineralization takes place both in the water column and in the sediments. Particulate matter has a sinking speed relative to the water and may accumulate on the bottom if the bottom stress is below a certain threshold value. Likewise, resuspension takes place if the bottom stress is above a limit. Parameterization of the biochemical processes is taken from literature based on experiments in laboratories and mesocosms, or deduced from field measurements (Pohlmann and Puls, 1994; Aksnes *et al.*, 1995; Mayer, 1995; Gehlen *et al.*, 1995; Lohse *et al.*, 1995, 1996). A comparison between some key characteristics and parameters between NorESM1-ME and NORWECOM.E2E is given in Table 1.

The incident irradiation used in the biochemical model is modelled using a formulation based on Skartveit and Olseth (1986, 1987) using short wave radiation outputs of the NorESM1-ME model, and corrected linearly at the sea surface using the modelled ice concentration. Initial fields for nutrients and DIC were interpolated from annual means of the NorESM1-ME simulation for the years 2001–2005, except for SI that has a large offset in the NorESM1-ME simulation with surface values close to 20 μM in the area of interest caused by advection of water with high SI from the Bering Sea. For SI typical winter values of Atlantic Water in the Norwegian Sea (SI = 5.5 μM, F. Rey, pers. comm.) were therefore used, together with some small initial amounts of algae (0.10 mg N m^{-3}) for both diatoms and flagellates. For DOC only the transient part is considered, and the initial value is therefore set to zero. These values are also used at the

Table 1. Comparison of some model characteristics for NorESM1-ME and NORWECOM.E2E.

	NorESM1-ME	NORWECOM.E2E
Nutrients	Nitrate, phosphate, silicate, iron	Inorganic nitrogen, phosphate, silicate
Phytoplankton	One bulk	Diatoms and flagellates
Zooplankton	One bulk	Micro and meso
P:N:C stoichiometry	1:16:122	1:16:112
POC remineralization rate (day^{-1})	0.03	0.0005, 0.0007, 0.0002 for N, P, and Si
DOC remineralization rate (day^{-1})	0.004	0.028 (transient part) at 0°C
Max phyto growth rate at 0° (day^{-1})	0.60	1.32 (dia), 0.88 (fla)
Max zoo growth rate (day^{-1})	1.0	0.27 (meso), 0.33 (micro) at 0°C

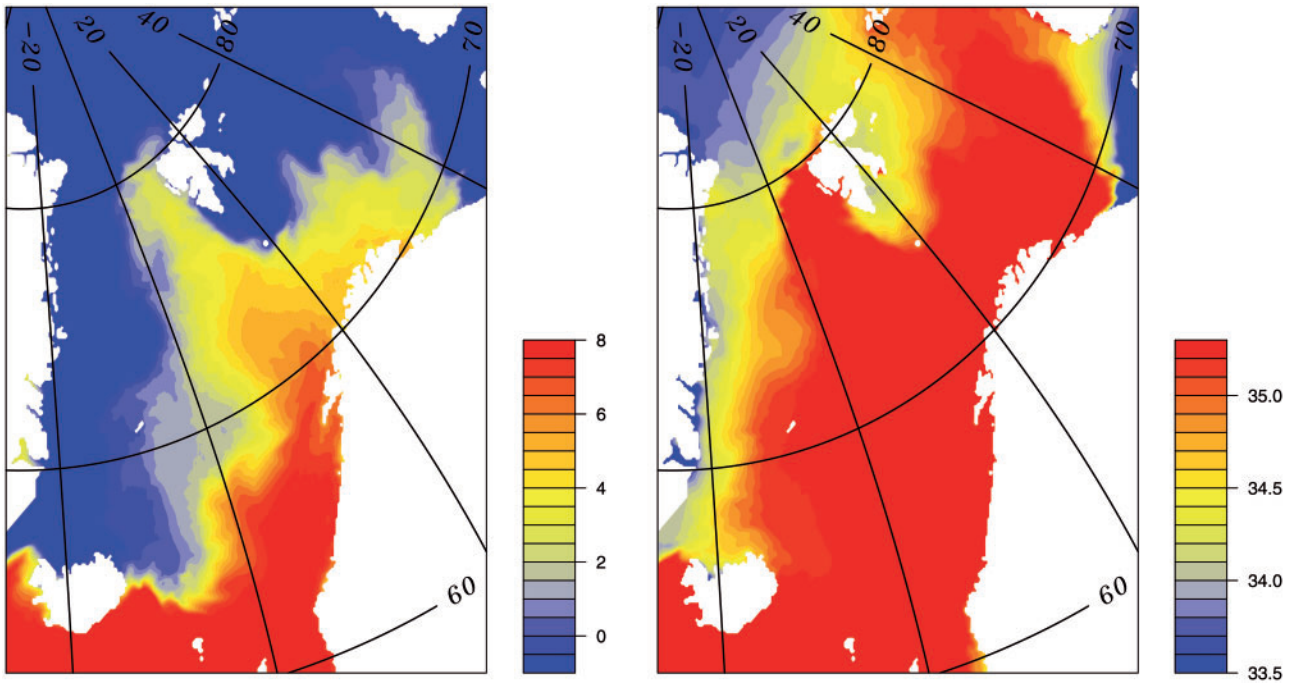

Figure 2. Mean temperature (left) and salinity (right) for January 2006 from the ROMS model.

open boundaries. Inorganic nitrogen is added to the system from the atmosphere, while there are no river inputs of nutrients and carbon. To absorb inconsistencies between the forced boundary conditions and the model results, a 7 gridcell "Flow Relaxation Scheme" (FRS) zone (Martinsen and Engedahl, 1987) is used around the open boundaries. The simulation started on 1 January 2006. After a 12 year spin-up (running the first year 12 times) the full model period (2006–2070) was run sequentially.

Results

Mean surface temperature and salinity for January 2006 are shown in Figure 2. As ocean physics is an input to the NORWECOM.E2E system, these results are from the ROMS downscaling (Sandø *et al.*, 2018), and since the ROMS downscaling was initiated from the global model 1 January 2006, the figures are close to the initial field and similar in both models. The temperature field clearly shows how the warm water is transported with the Norwegian Coastal Current northwards into the Barents Sea and west of Spitsbergen. Surface salinity is well above 35 in most of the Barents and Norwegian seas, while water below 34 is only found in the Arctic Ocean, in the Greenland fjords and in the southeastern Barents Sea.

Time series of annual mean sea surface temperature (SST) and salinity (SSS) for the Barents, Greenland and Norwegian seas (see Figure 1 for area definitions) for both the regional and global models are given in Figure 3. There is a general agreement on the magnitude between the two models in the Norwegian and Greenland seas SST, while the Barents Sea temperature is lower in the global (NorESM1-ME) than in the regional model. Using the Fitting Generalised Linear Models routine in R (glm), the trend in annual mean SST for the whole period has been computed. Except for the regional Greenland Sea, there is an increase in SST with the trend close to $0.02^{\circ}C\,year^{-1}$, with a slightly stronger increase in the global model. There is a positive SST correlation between regional and global models in the Barents and Norwegian seas ($r \approx 0.5$, $p < 0.01$), while SST is negative correlated in the Greenland Sea. The regional model is initialized from the global one, and there is an adjustment in SSS over the first decade of the simulation. In the Barents Sea the SSS increases rapidly before a similar decrease is seen. In the Greenland Sea SSS increases from 34.6 to 35.0, while in the Norwegian Sea there is similar decrease

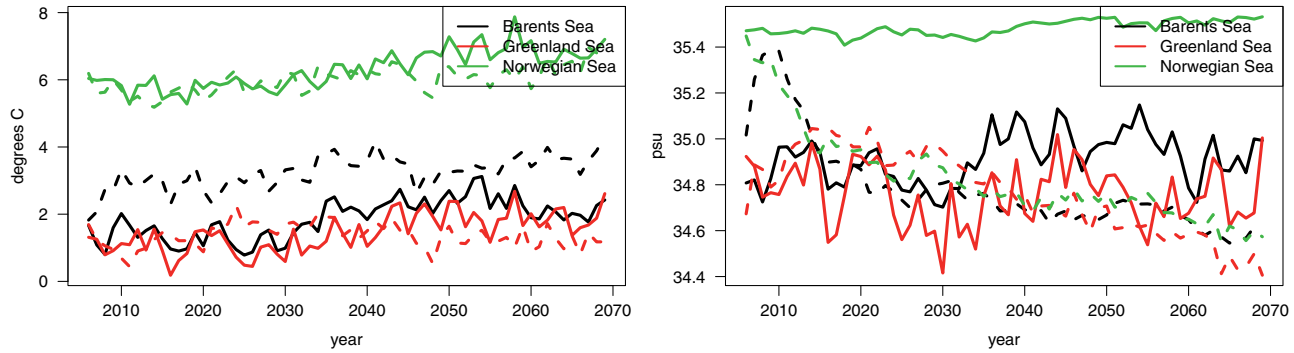

Figure 3. Annual mean sea surface temperature (SST, left) and salinity (SSS, right) for Barents Sea (black), the Greenland Sea (red), and the Norwegian Sea (green), for NorESM1-ME (solid line) and ROMS/NORWECOM.E2E (dashed line). Color refer to online version.

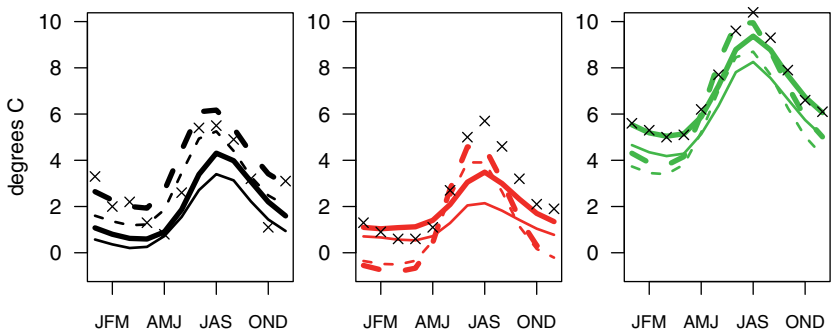

Figure 4. Annual cycle of sea surface temperature (SST) for the first (thin line) and last decades (thick line) for Barents Sea (black—left panel), the Greenland Sea (red—mid panel), and the Norwegian Sea (green—right panel), for NorESM1-ME (solid line) and ROMS/NORWECOM.E2E (dashed line). The *X-es* are the monthly means from the World Ocean Atlas for the period 2005–2012. Color refer to online version.

from 35.4 to 35.0. After this initial adjustment there is a steady decrease in the regional model ($\sim$0.007 year^{-1}) in all seas, while there are no trend in SSS in the global model.

The annual cycle of SST is shown in Figure 4, and statistics where the annual cycles of the first 10 years are compared with that from the World Ocean Atlas (WOA) are given in Table 2. It is clear that the temperature increases from the first to the last 10 year periods. Comparing the global and regional models, the spring warming starts earlier in the regional model than in the global one. Summer maximum occurs in both models in August, and the summer maximum is higher in the regional model. The figure also show that the seasonal amplitude is larger in the regional model than in the global one, and that this amplitude is higher in the last decade than in the first. This increase in amplitude is up to 0.87°C for the regional model in the Greenland Sea.

Time series of the annual mean upper 10 meters nutrients are shown in Figure 5. It is clearly seen that the values are much higher in the global than in the regional model, with a factor of 2 for inorganic nitrogen and PHO and a factor of four for SI (not shown). There is a small negative trend in the NorESM1-ME model value, and a positive correlation ($r \approx 0.4$, $p < 0.01$) between PHO and SI in the Greenland Sea as well as the Norwegian Sea. The explanation for the large offset between the annual mean values is seen in Figure 6 where the seasonal cycle for inorganic nitrogen is shown. Some statistics where these seasonal cycles of the first 10 years are compared with that from the WOA are also given in Table 2. The figure shows that the winter values are close between the models, while there are large differences in the levels

Table 2. Mean value, root mean square error (RMSE), and model bias of the seasonal cycle ($N = 12$) for the first 10 years (2006–2015) of sea surface temperature (Figure 4) and inorganic nitrate (Figure 6) for the two models compared with the observations from the World Ocean Atlas.

	Sea surface temperature			Inorganic nitrate		
	Mean	RMSE	Bias	Mean	RMSE	Bias
BSEA-WOA	2.9			3.4		
BSEA-NORWECOM	2.8	0.9	0.2	7.0	4.3	−3.6
BSEA-NorESM	1.5	1.8	1.5	10.8	7.4	−7.4
GSEA-WOA	2.5			7.1		
GSEA-NORWECOM	1.1	1.5	1.4	7.6	2.5	−0.4
GSEA-NorESM	1.1	1.8	1.3	12.3	5.7	−5.1
NSEA-WOA	7.1			7.1		
NSEA-NORWECOM	5.6	1.5	1.5	6.1	2.2	1.0
NSEA-NorESM	5.8	1.3	1.2	11.4	4.8	−4.3

the rest of the year. The regional model utilizes all available nutrients in the upper 10 m, while there are large amounts of excess nutrients in the global model, consistent with the lower GPP. The seasonal cycles confirm the negative trend in annual means for the global model. Similar to the maximum in SST, the summer minimum in surface nutrients occur at the same time in NORWECOM.E2E and NorESM1-ME, and the decline in spring starts earlier in the regional model.

Maps of annual mean primary production for both models averaged over the first decade of the simulation (2006–2015) are

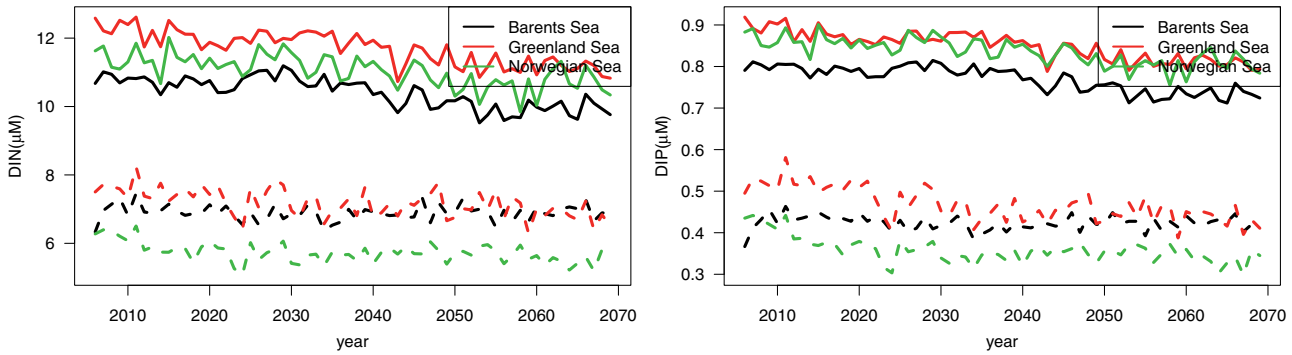

Figure 5. Long term annual mean (0–10 m) inorganic nitrogen (left panel) 1s and, phosphorous (right panel) for Barents Sea (black), the Greenland Sea (red), and the Norwegian Sea (green), for NorESM1-ME (solid line) and NORWECOM (dashed line). Color refer to online version.

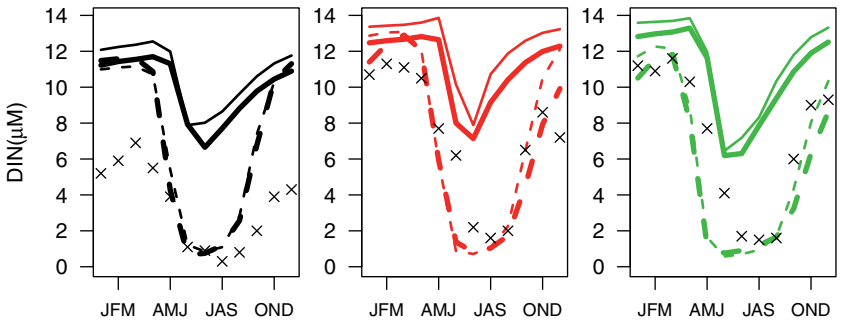

Figure 6. Annual cycle (0–10 m) of inorganic nitrogen for the first 10 years (thin line) and last 10 years (thick line) for Barents Sea (black—left panel), the Greenland Sea (red—mid panel), and the Norwegian Sea (green—right panel), for NorESM1-ME (solid line) and NORWECOM (dashed line). The *X-es* are the monthly means from World Ocean Atlas. Color refer to online version.

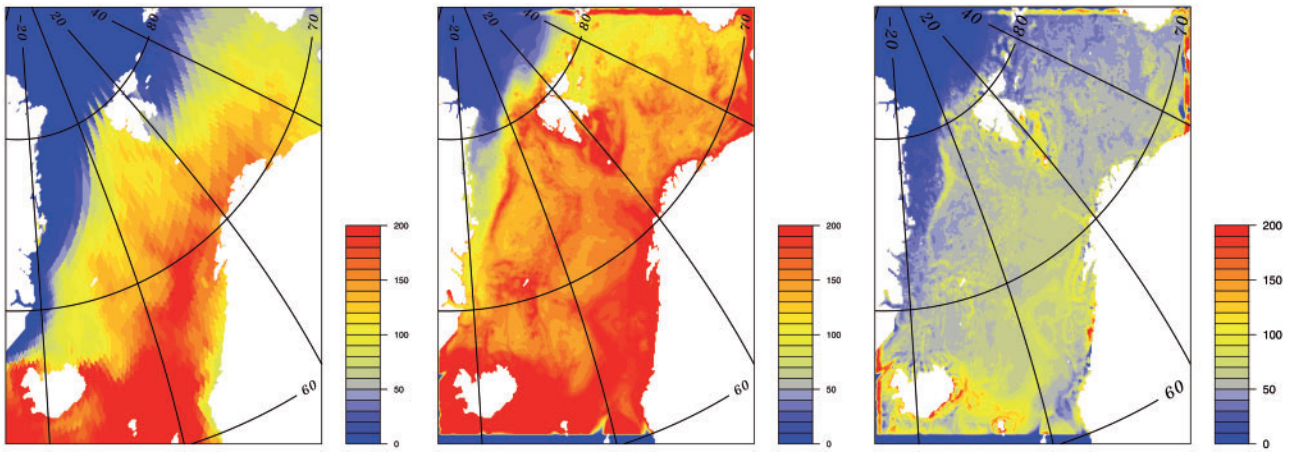

Figure 7. Annual mean primary production (gC m^{-2} $year^{-1}$) for the first decade (2006–2015). NorESM1-ME gross primary production (left), NORWECOM.E2E gross primary production (centre), and NORWECOM.E2E net primary production (right).

given in Figure 7. The gross primary production (GPP) is highest in the core of the warm Atlantic water in the Atlantic Current with lower values to the north and to the west. Comparing the two models, the GPP are generally higher in NORWECOM.E2E than in NorESM1-ME. This is most evident along the Greenland coast and in the northern Barents Sea, where the production in the global model is close to zero due to higher sea ice concentration in this model than in the regional (zero production along the southern boundary and high values to the northeast in the regional model is a boundary effect). In the last panel of Figure 7, annual mean net primary production (NPP) for the regional model for the same period is shown. The patterns are very similar to that of GPP, but the magnitude is much lower. On average, GPP in the regional model is 2.5 times higher than for the NPP. For GPP the mean values are 73, 68, and 139 g Cm^{-2} y^{-1} for NorESM1-ME in the Barents, Greenland, and Norwegian Sea, respectively, whereas the corresponding values for NORWECOM.E2E is 144, 154, and 180 g Cm^{-2} y^{-1}. For NORWECOM.E2E NPP, the values for the

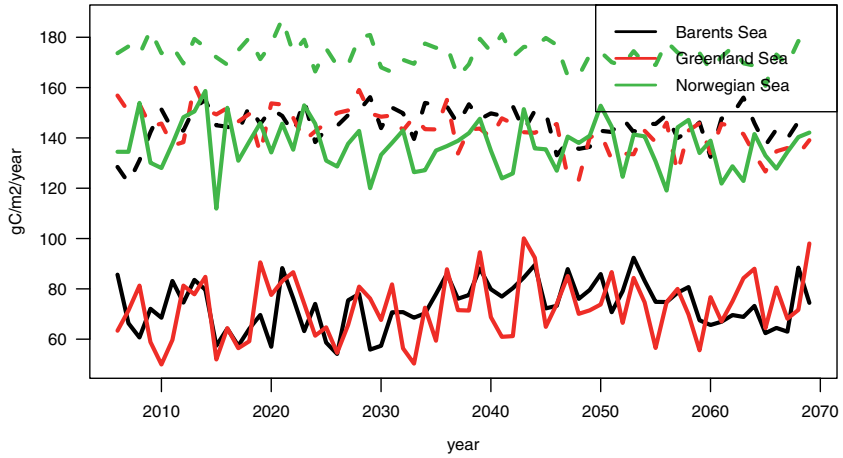

Figure 8. Annual mean gross primary production (GPP) for Barents Sea (black), the Greenland Sea (red), and the Norwegian Sea (green), for NorESM1-ME (solid line) and NORWECOM (dashed line). Color refer to online version.

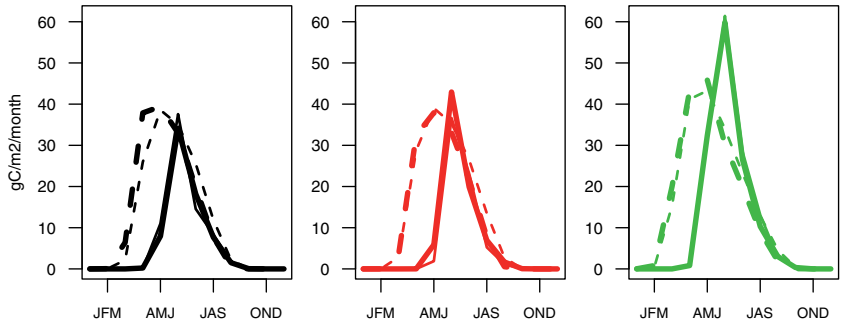

Figure 9. Annual cycle of gross primary production (GPP) for the first 10 years (thin line) and last 10 years (thick line) for Barents Sea (black—left panel), the Greenland Sea (red—mid panel), and the Norwegian Sea (green—right panel), for NorESM1-ME (solid line) and NORWECOM (dashed line). Color refer to online version.

same three domains are 54, 57, and 68 g Cm^{-2} y^{-1}. Time series of annual GPP is given in Figure 8. In the Barents and Greenland seas, GPP is a factor two higher in the regional than in the global model, while in the Norwegian Sea the models are closer. There is no significant correlation in GPP between the models, but within each model and between the seas the correlation is in the range $r = 0.3$–0.4 ($p < 0.01$) for all combinations of seas. No clear trend in any of the models or seas are found. Maximum trend (absolute level) is found for the regional model in the Greenland Sea with a long term decline of -0.08 g Cm^{-2} y^{-1}. A comparison of the GPP seasonal cycle (Figure 9) is consistent with that of the temperature and nutrient ones. The spring bloom in the regional model is earlier than for the global model (Figure 9), whereas the end of the production season is in all regions and models the same (August/September). In NORWECOM.E2E the production maximum is in May, while in NorESM1-ME the maximum is in June. The difference in the timing and maximum GPP between the two models can be attributed by the difference in the phytoplankton growth rate parameterizations, which is calibrated differently.

Maps of annual mean pH in the upper 10 m for both models and averaged over the first decade of the simulation (2006–2015) are given in Figure 10. The magnitude is generally higher in NorESM1-ME (mean value 8.13 compared with 8.08), while the regional differences is more pronounced for NORWECOM.E2E, especially with lower pH levels along the Norwegian and the Greenland coast. There is a steady decline in pH in both models (see Figure 11, left panel), with a negative trend between -0.0021 and -0.0025 $year^{-1}$ for both models and all three seas. The pH is slightly higher in the global model than in the regional one by a mean of 0.03 in Barents and Greenland seas and 0.05 in the Norwegian Sea. The results are similar for the saturation level of aragonite, Ω_{ar} (see Figure 11, right panel). In the global model the levels are slightly higher (0.1, 0.2, and 0.3 in Barents, Greenland, and Norwegian seas, respectively), with negative trends for both models close to -0.007 $year^{-1}$.

Spatial maps for annual CO_2 flux for the first decade (2006–2015) are shown in Figure 12. The flux is higher in NorESM1-ME (10.69 compared with 5.75 mmol m^{-2} day^{-1} averaged over the whole area), while the regional differences is larger in NORWECOM.E2E. Maximum uptake of CO_2 is in both models >20 mmol m^{-2} day^{-1} in parts of the Greenland Sea. While the global model has a net uptake of CO_2 in the whole area, the regional model act as a source of CO_2 in the Arctic and along the Greenland and Norwegian coasts. Time series in annual CO_2 flux for the three different seas are shown in Figure 13. Both models suggest that the uptake is largest in the Greenland Sea. While the fluxes are similar between the seas for the NorESM1-ME model, there are large regional differences in the regional model ranging

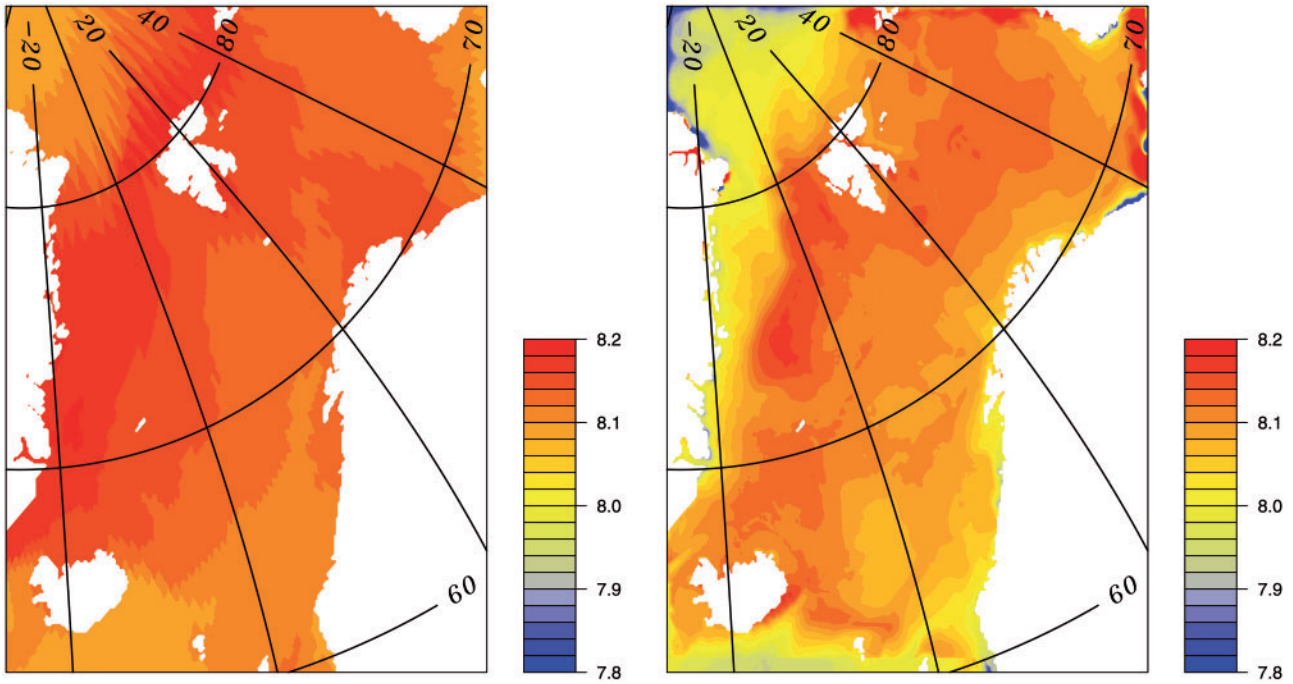

Figure 10. Annual mean pH (0–10 m) for the first decade (2006–2015). NorESM1-ME (left) and NORWECOM (right).

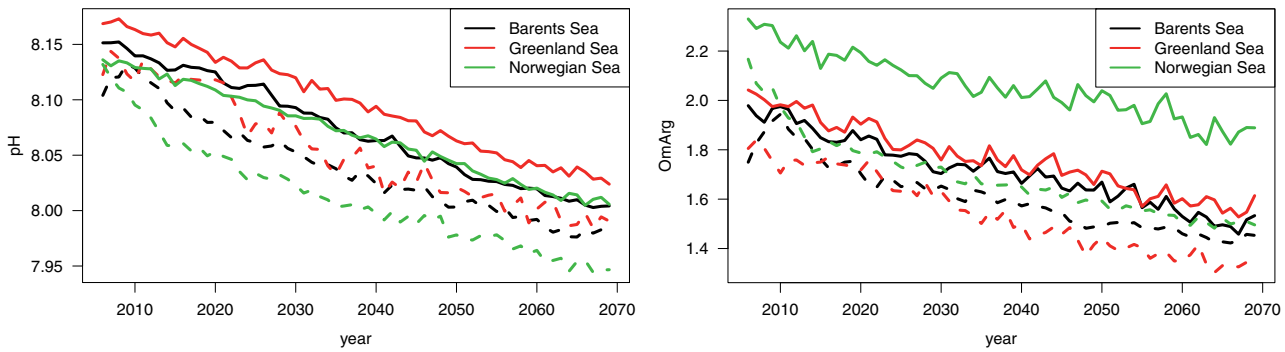

Figure 11. Annual mean (0–10 m) pH (left panel) and Ω_{ar} (right panel) for Barents Sea (black), the Greenland Sea (red), and the Norwegian Sea (green), for NorESM1-ME (solid line) and NORWECOM (dashed line). Color refer to online version.

from $<5\,\mathrm{mmol\,m^{-2}\,day^{-1}}$ in the Norwegian Sea to almost $15\,\mathrm{mmol\,m^{-2}\,day^{-1}}$ in the Greenland Sea. There is a positive trend (increasing uptake) in the flux in the global model with a maximum of $0.06\,\mathrm{mmol\,m^{-2}\,day^{-1}\,year^{-1}}$ in the Greenland sea, whereas NORWECOM.E2E give a positive trend in the Greenland sea ($0.04\,\mathrm{mmol\ m^{-2}\,day^{-1}\,year^{-1}}$), a negative trend in the Norwegian Sea ($-0.03\,\mathrm{mmol\ m^{-2}\,day^{-1}\,year^{-1}}$) and only a slight decrease in the Barents Sea ($-0.005\,\mathrm{mmol\,m^{-2}\,day^{-1}\,year^{-1}}$). Averaged over the whole area, there is an increase in the uptake of CO_2 in NorESM1-ME of 9% and NORWECOM.E2E of 7% from 2006 to 2070. The most prominent features in the seasonal cycle (see Figure 14) is the large positive flux during winter in the Greenland Sea, and the shift in season for the regional model in the Barents and Norwegian seas with lower winter values in the last 10 years than in the first period. The flux is always positive (ocean uptake) for both models, with the lowest values in the Norwegian Sea in the last period for the NORWECOM.E2E. For both models the strongest seasonal cycle is found in the Greenland Sea.

Discussion

Validation of present day climate

Using data from WOA (https://www.nodc.noaa.gov/OC5/woa13/woa13data.html) (2005–2012 values) and averaging over the same areas give annual means of SST 2.9, 2.5, and 7.1°C for the Barents, Greenland, and Norwegian Sea, respectively, Table 2). In the Barents Sea the global model is too cold, while the regional model adjusts to the correct level after a ∼5 years. In the Greenland and Norwegian Seas, the global model is ∼1°C too cold. Here the regional model, which is initialized from the global one, has the same cold bias throughout the whole model period, due to too much vertical mixing. Except for the Barents Sea where the RMSE and bias is much lower in the regional model, the statistics for the annual cycle of the first 10 years are generally comparable for the two models. Comparing climatology of SSS from the WOA (34.5, 34.6, 35.0 for the Barents, Greenland, and Norwegian Sea, respectively), the NorESM1-ME is obviously much too saline in the Norwegian Sea, while the two other seas

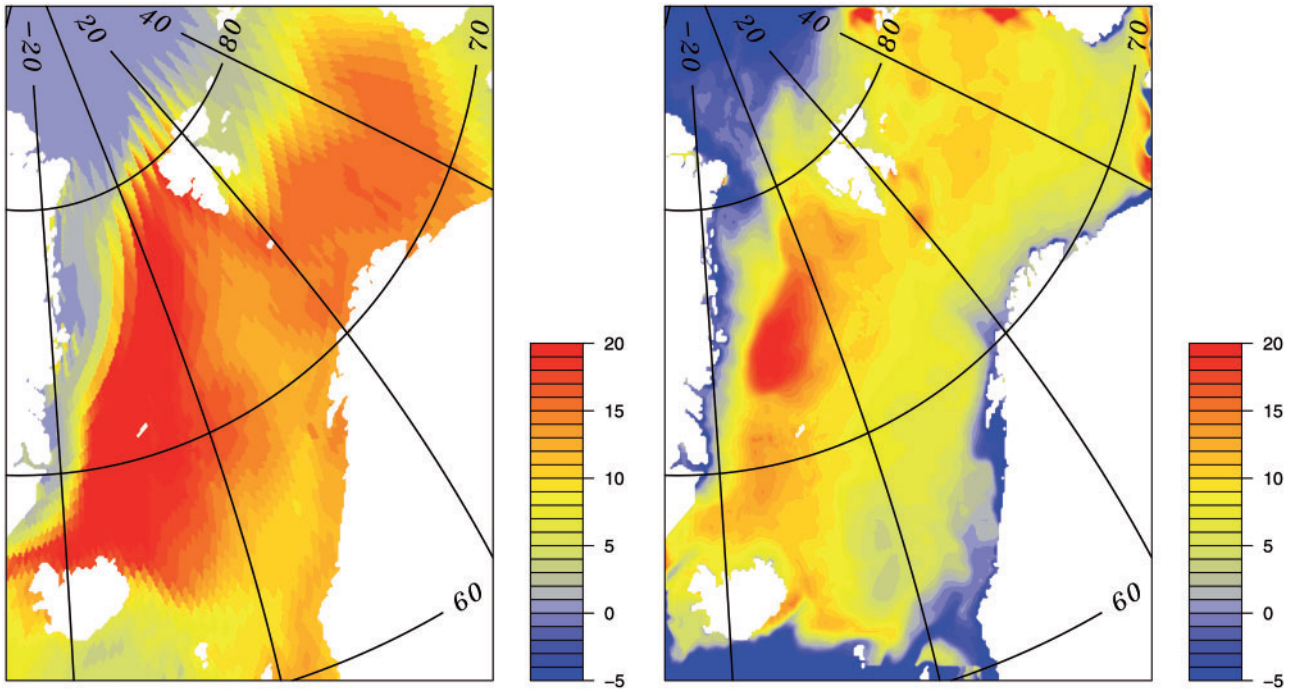

Figure 12. Annual mean air–sea CO_2 flux (mmol m^{-2} day^{-1}) for the first decade (2006–2015). NorESM1-ME (left) and NORWECOM (right). Positive values are uptake.

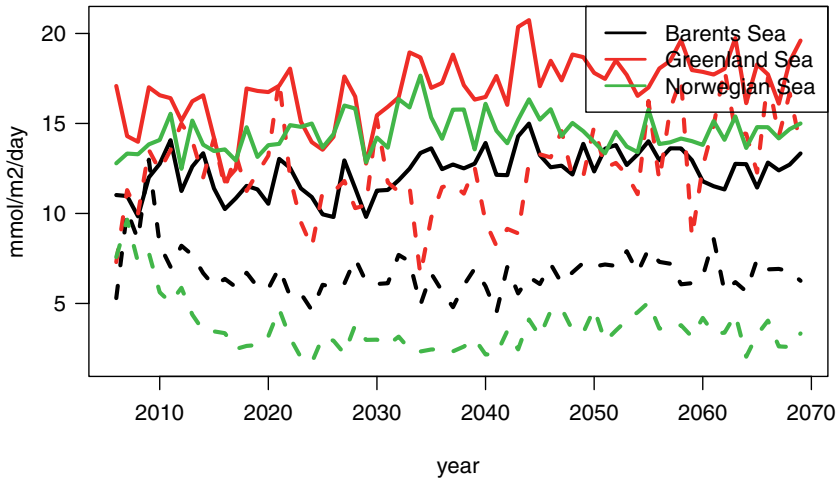

Figure 13. Annual mean CO_2-flux for Barents Sea (black), the Greenland Sea (red), and the Norwegian Sea (green), for NorESM1-ME (solid line) and NORWECOM (dashed line). Color refer to online version.

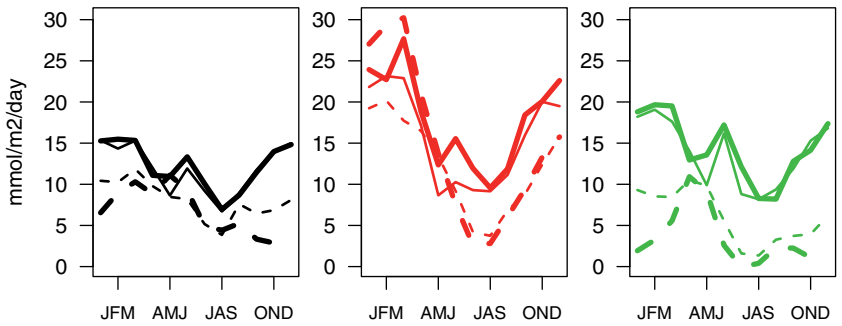

Figure 14. Annual cycle of CO_2-flux for the first 10 years (thin line) and last 10 years (thick line) for Barents Sea (black—left panel), the Greenland Sea (red—mid panel) and the Norwegian Sea (green—right panel), for NorESM1-ME (solid line) and NORWECOM (dashed line). Color refer to online version.

also have a positive bias. The regional model uses the first 5–10 years as spin-up to adjust the initial field. After this period a decreasing trend is bringing the SSS closer to a more realistic level over the simulation period, but the model never seems to stabilize at correct levels. Focusing on the seasonal cycle in SST (see Figure 4), the modelled maximum temperature in August and minimum in March is in accordance with the observations. The annual temperature amplitude is largely underestimated in the global model, while there is a good correspondence between the regional model and the observations.

As already stated, the SI values in NorESM1-ME is unrealistically high. Comparing with the WOA, this is also the case for inorganic nitrogen and PHO. Omitting some small regional differences, the modelled annual mean inorganic nitrogen from the global model is close to 11 μM, whereas PHO is around 0.8 μM. The corresponding observations from WOA are 3.4, 7.1, and 7.1 μM for inorganic nitrogen for the Barents, Greenland, and Norwegian Sea, respectively, Table 2), and 0.4, 0.6, and 0.5 μM for PHO. Except for an overestimate in inorganic nitrogen in the Greenland Sea, the regional model has better fit to the observed annual means, despite being initialized from NorESM1-ME and using these values (N and P) on the open boundaries. An explanation of the discrepancies between the global model and observations are seen in the seasonal cycle of inorganic nitrogen in Figure 6. Except for the Barents Sea, there is a good agreement between both the models and the observed winter values. The difference in the annual means is due to the fact that when the NORWECOM.E2E model is able to utilize all available nutrients and bringing summer minimum close to zero in accordance with observations, the minimum in NorESM1-ME is around 6 μM. The reason for non-exhaustive nutrient consumption in NorESM1-ME in summer is because of a balance between further use of nutrients from phytoplankton growth, and the sources of new nutrients through remineralization of phytoplankton and zooplankton, the decay of DOC and remineralization of detritus. Here, the additional constraint on phytoplankton growth by zooplankton grazing (Table 1) dominates over nutrient re-supply predominantly by remineralization of detritus. The timing of the decline in surface nutrients in spring corresponds between the regional model and the observations, while the global model is delayed. However, the decline is faster in the regional model than observed so that the summer minimum is reached in June/July compared with the observed minimum in August. These findings are also confirmed from the RMSE and bias in Table 2, as the results from NORWECOM is much better than those from NorESM1-ME in all three domains.

The study areas cover a large area south and north of the Arctic Circle, on both sides of the Arctic Front. Therefore, phytoplankton is exposed to wide variations in physical forcing factors such as light, temperature, and nutrient supply, which combined control the growth rate. To estimate the annual primary production under such conditions is almost impossible mainly for logistical reasons that result in a scarcity of measurements. Nevertheless, through combining existing measurements in the Norwegian Sea, an annual NPP rate of $\sim$80 g C m^{-2} y^{-1} has been estimated (Rey, 2004). Annual NPP in the Greenland sea are apparently comparable with those in the Norwegian Sea, and estimated to be $\sim$70 g C m^{-2} y^{-1} in Rey *et al.* (2000) and 81 g C m^{-2} y^{-1} in the open Greenland Sea by Richardson *et al.* (2005). In the Barents Sea, estimates of primary production varies a lot between the different water masses. Titov and Orlova (2011) give a mean value for GPP in the Barents Sea of 111 g C m^{-2} y^{-1}, while Slagstad *et al.* (2011), using the SINMOD model, give a value of 102 g C m^{-2} y^{-1} (GPP) and 53 g C m^{-2} y^{-1} (NPP). The NPP in NORWECOM.E2E is at comparable magnitude to observations in both the Greenland and Norwegian seas, whereas in the Barents Sea, NPP is in agreement with the SINMOD model, while GPP is somewhat high. For NorESM1-ME, where only GPP is available, the values are obviously too low in the Barents and Greenland seas while in the Norwegian Sea (assuming a similar NPP:GPP ratio as for SINMOD and NORWECOM.E2E), the values are close to observations. Recalling the large reservoir of available summer nutrients in the global model, this seems consistent with the low production in the Barents and Greenland seas, however using the same argument in the Norwegian Sea would result in an annual primary production far above other estimates.

Time-series observations from Ocean Weather Station Mike (OWSM) at (66°N, 2°E) in the Norwegian Sea, have shown that the pre-bloom starts early March (average on 2 March), and that the time at which the bloom reaches its peak can vary by as much as 5–6 weeks from year to year. The observations indicate that the average time of the peak spring bloom is May 21st (mean for 1991–2003) and that the production season lasts until October. Maximum observed chlorophyll$_a$ concentration in spring is barely >3 mg Chla m^{-3} (Rey, 2004). In the Greenland Sea, Richardson *et al.* (2005) make a summary of several studies and conclude that the spring bloom starts in March, maximum production occurs in May/June and that there still is a significant production going on in August. On the basis of modelling and observations, Titov (1995) describes the seasonal dynamics of primary production in the Barents Sea. It starts already in March and develops first in Atlantic and coastal waters and peeks in May/June before it slows down in June/July. The zone of the spring bloom moves to the north and northeast along the ice edge. In late summer and fall a second bloom is seen in the western Barents Sea formed by inflow of nutrient-rich Atlantic water. Chlorophyll$_a$ observations along the Fugløya–Bjørnøya transect at the Barents Sea opening confirm this general picture with the pre-bloom starting in March, maximum chlorophyll$_a$ in June and a second peak in August (Dalpadado *et al.*, 2014).

Onset of the spring bloom the NORWECOM.E2E model is in all areas in March with peak primary production in May in agreement with observations. From September onwards the GPP is close to zero, thus the model gives a shorter season than the observations. In the NorESM1-ME model the production season is even shorter starting in May with peak production in June, while (similar to the regional model) GPP is close to zero from September. Reflecting the shorter season, maximum production rate is highest in the global model up to 60 gC m^{-2} month^{-1} in the Norwegian Sea in June. The timing of the spring phytoplankton bloom depends strongly on the physical conditions, especially the development of the upper mixed layer (e.g. Taylor and Ferrari, 2011). However, when comparing the physics between the models there are no variables that can explain the large differences in the onset of the spring bloom. Instead, this discrepancy between the models is due to the parameterization of the phytoplankton growth (see Table 1). The maximum production rate at 0°C is considerably larger in NORWECOM.E2E (1.32 day^{-1}) than in NorESM1-ME (0.60 day^{-1}), which allows the former model to reach earlier net positive growth rate and hence bloom period.

Using observation from 2001 to 2006 (monthly or higher frequency) from OWSM (Skjelvan *et al.*, 2008) mean pH and Ω_{Ar} in

the upper 10 m is estimated to 8.11 and 2.25, respectively. This is close to more recent observations (2012–2015) from a buoy operating at the same site reporting on minimum values of pH and Ω_{Ar} in winter around 8.06 and 1.85, increasing to 8.2 and 3.0 in summer (Chierici *et al.*, 2016). Lauvset *et al.* (2016) mapped pH from the GLODAPv2 (Olsen *et al.*, 2016) data set on a global $1^\circ \times 1^\circ$ grid using the DIVA software (Troupin *et al.*, 2012). On the basis of this, the average upper 10 m pH in the Barents, Greenland, and Norwegian seas are 8.11, 8.19, and 8.14, respectively. Compared with this, the global model is a little high in the Barents Sea, while the regional model is a little low in the Greenland Sea. Both models suggest the Norwegian Sea to have the lowest surface pH among the areas discussed, which contradicts the GLODAPv2 data set that has the lowest values in the Barents Sea. Also, the Ω_{Ar} can be computed from the GLODAPv2 data set. Using all available data points in the three boxes, the average values are 2.14, 2.01, and 2.32 for the Barents, Greenland, and Norwegian Sea, respectively. This suggests that Ω_{Ar} in the NorESM1-ME model is too low in the Barents Sea, while the NORWECOM.E2E has a low bias in all regions. Nevertheless, even if this is the most extensive data set available, the number of observations is limited. Between 1981 and 2013 the data base consists of 175 data points in the Barents Sea, 250 in the Greenland Sea, and 800 in the Norwegian Sea. Their seasonal and spatial coverage is limited and does not necessarily represent a full annual average in a regional sea. Mapping the observed pH and Ω_{Ar} at OWSM with the modelled mean from NORWECOM.E2E for the first five years (2006–2010) show that the model has an almost perfect match with pH = 8.12 and $\Omega_{Ar} = 2.18$.

The uptake of CO_2 (Figure 13) is in accordance with Chen and Borges (2009) who suggest that in general high-latitude continental shelf seas tend to be net annual sinks of atmospheric CO_2. Several estimates of the annual air–sea CO_2 flux for the Barents Sea exist based on different data sets and approaches, ranging from 3.5 to 12 mmol m^{-2} day^{-1} (Bates and Mathis, 2009; Lauvset *et al.*, 2013). Manizza *et al.* (2013) estimated the sink of CO_2 in the Barents and Greenland seas to be 4 and 2.3 mmol m^{-2} day^{-1} in the period 1996–2007 using a regional physical–biogeochemical model for the Arctic, while Skogen *et al.* (2014) report on present day (20C3M) CO_2 flux in the Barents Sea of 5.3 mmol m^{-2} day^{-1}. Using Self Organised Maps, Yasunaka *et al.* (2016) estimated monthly gridded ($1^\circ \times 1^\circ$) CO_2 flux in the whole Arctic for the period 1997–2003. In the Barents Sea the mean net sink was estimated to be 10 mmol m^{-2} day^{-1}, and in the Greenland and Norwegian Sea 11 mmol m^{-2} day^{-1}. The seasonal cycle shows a maximum sink in winter (February/March) of 12 and 15 mmol m^{-2} day^{-1}, respectively, and a minimum in summer (June/July/August) of ~5 mmol m^{-2} day^{-1}. The strong winter uptake in the Norwegian Sea in NorESM1-ME has been shown to be inconsistent with the data and likely as a result of the anomalously strong MLD bias rather than the biological processes (Gharamti *et al.*, 2017). In the Barents Sea, NorESM1-ME is in the high end of previous estimates, while NORWECOM is well within. Both models have a less pronounced seasonal cycle than reported by Yasunaka *et al.* (2016). Nevertheless, there are large spatial differences (Figure 12) in both models. Recalculating both the annual mean and seasonal cycle in the NORWECOM.E2E model using the exact same boundaries as Yasunaka *et al.* (2016), gives a different picture. During the first decade the annual means for the Barents and Greenland/Norwegian (considered as one area) seas are 7 and 8 mmol m^{-2} day^{-1}, respectively. There is also a clear seasonal cycle with winter maxima of 10 and 13 mmol m^{-2} day^{-1} and summer minima of 5 and 2 mmol m^{-2} day^{-1}.

Future climate changes

Future changes in the downscaled physics in the Barents Sea has been studied in Sandø *et al.* (2018). There, to study a possible realization of the climate 50 years from now, the model mean values for the decade 2010–2019 was subtracted from the last decade 2060–2069. The downscaled model results show an increase in temperatures of ~0.5–1 °C in most parts of the Barents Sea, somewhat more along the Polar Front in the Hopen Trench and in the northeastern parts of the Barents Sea in March (winter/spring), and somewhat less in September (summer/autumn), with a slight cooling in the southeastern parts. Reductions in sea ice extent reflects the increased temperatures and are most prominent in the northern Barents Sea, specifically along the northwestern coast of Novaya Zemlya and in the Barents Sea Exit, but also along the coast in the southeastern Barents Sea where sea ice is present during March. The inter-annual and decadal variability is quite substantial and bigger than the overall trend during the simulation period.

There are no changes in future nutrient levels, and neither the global nor the regional model indicate any changes in the primary production at regional level. In general terms high-latitude spring-bloom ecosystems should benefit from increases in temperature giving increased regenerated production, but other factors like changes in mixed-layer-depth may alter this. The present study adds to other modelling studies that reports on the effect of climate change on primary production in the area, without any general agreement on how this will be effected. Steinacher *et al.* (2010) suggest a significant increase in primary production in 2100 under the A2 emission scenario based on an ensemble of 4 global models. Using a slightly different set-up of the NORWECOM model, Skaret *et al.* (2014) predicts a strong increase in primary production in the Barents Sea in 2065 under A1B using a regional downscaling of the GISS-AOM global climate model, while Slagstad *et al.* (2015) predicts a general decrease in primary production except for areas where ice retreats in 2100 under A1B using the SINMOD model and climate forcing from MPI-ECHAM5. Using POLCOMS-ERSEM forced by IPSL-CM4 under A1B, Barange *et al.* (2014) predicts a strong increase in phytoplankton biomass in the Greenland and Jan Mayen Economical exclusive economic zones (EEZs) and a slight decline in the Norwegian EEZ in 2050.

The average pH of the surface waters of the global oceans has decreased from ~8.2 before the onset of the industrial revolution to a present average of ~8.1 (Caldeira and Wickett, 2003; Orr *et al.*, 2005). Over the last quarter century the decrease has been by a rate of ~0.0018 yr^{-1} at several open-ocean time-series sites (Feely *et al.*, 2009). Lauvset *et al.* (2015) report on a decrease in the surface pH in the North Atlantic subpolar seasonally (NASPSS) biome of -0.0020 ± 0.0004 yr^{-1} between 1991 and 2011 using data from SOCAT collection (www.socat.info). Olafsson *et al.* (2009) report an even higher rate of -0.0024 yr^{-1} in the Iceland Sea for the period 1985–2008, thus the decline in pH in both models (on average -0.0024 yr^{-1}) is within these observations. At the end of the century (2080–2100), the IPCC reports the global mean surface pH to decrease to 7.97 under RCP4.5 (Figure 2.5 in IPCC, 2014). This represents a decline of 0.14–0.15 compared with the level in 1986–2005. Using the modelled rate over a

75 year period (1995–2070) the models suggest a decrease in surface pH of 0.18. As the increase in atmospheric CO_2 is low after 2070 under RCP4.5, and the decline in pH is believed to be even stronger in the Arctic, the modelled rate of future change in surface pH is in accordance with this prediction.

A large proportion of marine life forms incorporate calcium carbonates in body armour, and ocean acidification leads to less favourable conditions for the formation of these minerals. Current surface seawaters are generally supersaturated with respect to calcium carbonates ($\Omega > 1$), but saturation state decreases when more CO_2 is dissolved in the water (reduced pH). A decrease in the carbonate concentration will thereby affect the survival of calcifying organisms, and when the carbonate concentration reaches a critical level the seawater will become corrosive for the calcifying organisms (Roleda *et al.*, 2012). Changes in saturation state with respect to these minerals are therefore important for understanding how ocean acidification might impact future ecosystems. In 2002 the observed saturation horizon of aragonite ($\Omega_{ar} = 1$) in the Norwegian and Greenland Seas was ~2000 m (Børsheim and Golmen, 2010 based on Olsen *et al.*, 2006). Compared with observations from 1981, there had been a shoaling of 150 m (or 7 m year^{-1}). In the Iceland Sea Olafsson *et al.* (2009) report on a shoaling rate of 4 m year^{-1} in the period 1985–2008. Initially, undersaturation of Ω_{ar} in the Norwegian and Greenland seas appears below 3600 m in the regional model (not shown). At the end of the simulation the saturation horizon in these areas was ~2600 m. This gives a shoaling of the saturation horizon of ~1000 m in 64 years (16 m year^{-1}). From an ensemble of climate models, Orr *et al.* (2005) report on the shoaling of the saturation horizon of aragonite in future climate. Following the IS92a emission scenario (723 ppm in 2100, which is slightly more pessimistic than RCP4.5 until 2060 when RCP4.5 stabilizes while IS92a continue to increase steadily) the annual average aragonite saturation shoaling in the North Atlantic (north of 50°N) during the 21st century, is 25 m year^{-1}. The present shoaling from the regional downscaling is thereby well within the mean of the observed and predicted rates.

The exchange of CO_2 between atmosphere and seawater is relatively rapid with an equilibrium time scale of a year (Broecker and Peng, 1974), so that CO_2 in surface waters in most ocean regions increase from year to year in proportion to the increased CO_2 concentration in the atmosphere. However, there are several climate feedbacks related to the oceanic uptake of CO_2. First higher temperature will increase the partial pressure of CO_2 in the surface water and thereby reduce the ocean uptake. Second, climate change will have an effect on convective mixing and density stratification, which also will have an effect on the transport of CO_2 into the ocean interior, and finally climate change will alter the natural carbon cycling through changes in biological production (Matear and Hirst, 1999). Averaged over the whole area, both models report on increase in ocean CO_2 uptake (7% for the regional model and 9% for the global one). The increased SST will decrease the ocean uptake of CO_2. As the biological production is approximately unchanged in the model both with respect to timing and magnitude, the increased uptake must be due to a positive contribution from changes in convective mixing and density stratification. For the regional model the increased uptake is strongest in the winter in the Greenland Sea (Figure 14). For the Barents Sea the regional model suggests a slight decrease in CO_2 uptake. This is in disagreement with Skogen *et al.* (2014) who estimated an increase in the Barents Sea CO_2 uptake from 5.3 to 8.5 mmol m^{-2} day^{-1} between 2000 and 2065 under emission scenario A1B. In their study, the main driver for this change was a change in DIC, which mainly contributed from a strong increase in the modelled primary and secondary production in the future climate, an increase that is not found in the present study.

Concluding remarks

The biogeochemistry from a global climate model (NorESM1-ME) has been compared with results from a regional model (NORWECOM.E2E) forced by a downscaling of the same climate simulation using the ROMS model. The focus has been to validate and determine the long term changes at regional scales, as the regional model obviously resolves local details that are not seen in the global model. The study concludes that the global model is able to reproduce several of today's observations on a regional scale, but that there are many spatial details that are lost when a coarse resolution global model is used. The global model has a cold (in summer) and saline bias compared with climatology in the areas discussed, a bias that the regional model is able to alleviate to some extent. SI is unrealistically high in the global model, while winter values for inorganic nitrogen and PHO are close to the observations. On the other hand, the summer nutrient minimum is too high, as the global model is not able to utilize all nutrients in the upper layers, in contrast to the regional model. This results in a primary production in the Barents and Greenland seas below previous observational-based estimates, and a delayed onset of the spring bloom. The regional model is more reliable at projecting production level and timing, but the spring bloom develops too fast. Both models are comparable to the observations for pH and Ω_{Ar}, while NorESM1-ME is in the high end of CO_2 flux estimates. There is a general agreement between the two models on future predictions, except for the development in SSS. There is no trend in future NPP in any of the models, while the trends in modelled pH and Ω_{Ar} are the same in both models. The largest discrepancy is in the development of the uptake of CO_2, where the regional model suggests a slight reduced uptake in the future. Overall, when assessing present day climate impact on marine biogeochemistry and ecosystem, we demonstrate that a spatially coarse IPCC-class Earth System Model underperforms the regional model.

One can argue that since the two applied biogeochemical models are different in their structure and parameterization, it is not only differences in scales (model resolution) and physical patterns, but also the inherent properties of the model formulations that contribute to the simulated differences. This problem was investigated by Skogen and Moll (2005) following up a previous study comparing two biogeochemical models in the North Sea (Skogen and Moll, 2000). In the first study it was shown that the two models agreed on annual mean primary production, its variability and the timing and size of the peak production. On the other hand, there was a low (even negative dependent of area) correlation in the production in different years between the two models. In the second study, the experiment was repeated, but both biogeochemical models were forced by the same physical model. The results were that the correlation between years became positive (changing from $r = -0.49$ to $r = 0.63$ for the North Sea annual production), and it was concluded that the single most important factor for a reliable modelling of phytoplankton and nutrient distributions and transports was a proper physical model. However, in addition to bias associated with poorly resolved physical processes, bias in the simulated seasonal cycle in

key biogeochemical state variables are also attributed to the over-simplified ecosystem parameterization in the NorESM1-ME model, with a relatively slow phytoplankton growth compared with the grazing efficiency from zooplankton (Table 1). Data assimilation with the same global biogeochemical model (HAMOCC) indeed suggests that considerably model-data misfit in the seasonal cycle can be alleviated with a regional-varying ecosystem parameterization (Tjiputra *et al.*, 2007).

Nevertheless, when interpreting the results, several limitations should be taken into account. Models can only produce results, which are already predetermined by the model equations. As an example, climate change can favour other plankton groups than those included in the model and thereby potentially shift the ocean's ability to serve as sink of CO_2. The regional model is forced by downscaled ocean physics, but using atmospheric forcing from the global climate model. This might lead to, e.g. cold biases due to the insulation by the ice cover in the global model since the downscaled ocean physics has less sea ice in better correspondence with the observed ice extent (Sandø *et al.*, 2018). The present study is only using one future scenario (RCP4.5) and one realization of it through the NorESM1-ME climate model. This is a clear limitation and has to be taken into consideration when interpreting the results. Through the ENSEMBLES project (http://ensembles-eu.metoffice.com) it was recommended to use results based on two or more RCM that again are forced by at least two Global Climate Models for climate impact studies (ENSEMBLES, 2009). The present study should therefore be considered as one member of a future ensemble of studies on the consequences of climate change. Upcoming studies using other models will either strengthen or weaken the findings, and thereby form an evaluation of the realism in the present set-up.

Analysis of the uncertainty of a future projection in the context of global models is well illustrated by the work of Hawkins and Sutton (2009). Uncertainty is built up of three aspects: scenario uncertainty (reflecting the unknown future socio-economic landscape), model uncertainty (reflecting inaccuracies in the model) and internal variability (reflecting the difficulty in detecting a clear climate change signal until this *averages out*). In their work it is demonstrated how model and internal variability uncertainty decrease with lead time, while scenario uncertainty increases. This is also the case in the present study, which shows an evolution of an initial value problem, where the initial field and model uncertainties dominate, to a boundary value problem, where the emission scenario and corresponding atmospheric CO_2 have the largest impact on the results. It is also demonstrated (Hawkins and Sutton, 2009), how, by moving from a global to a regional scale, the model and internal variability uncertainty can substantially increase. Therefore, single model simulations as forecasts of future conditions is questionable and should be viewed with an appropriate degree of caution.

Acknowledgements

This study was supported by the Centre for Climate Dynamics (SKD) in Bergen, Norway through the BIGCHANGE, PARADIGM, and LOES projects, and the FRAM centre in Tromsø, Norway through the Ocean Acidification Flagship. JT acknowledges Research Council of Norway through EVA (229771).

References

Aksnes, D., Ulvestad, K., Baliño, B., Berntsen, J., Egge, J., and Svendsen, E. 1995. Ecological modelling in coastal waters: towards predictive physical–chemical–biological simulation models. Ophelia, 41: 5–36.

Barange, M., Merino, G., Blanchard, J. L., Scholtens, J., Harle, J., Allison, E. H., Allen, J. I., *et al.* 2014. Impacts of climate change on marine ecosystem production in societies dependent on fisheries. Nature Climate Change, 4: 211–216.

Bates, N., and Mathis, T. 2009. The Arctic Ocean marine carbon cycle: evaluation of air–sea CO_2 exchanges, ocean acidification impacts and potential feedbacks. Biogeosciences, 6: 2433–2459.

Bellerby, R., Olsen, A., Furevik, T., and Anderson, L. 2005. Response of the surface ocean CO_2 system in the NordicSeas and North Atlantic to climate change. *In* The Nordic Seas: An Integrated Perspective, Geophysical Monograph Series, vol. 158, pp. 189–198. Ed. by H. Drange, T. Dokken, T. Furevik, R. Gerdes and W. Berger. American Geophyiscal Union.

Bellerby, R. G. J., Silyakova, A., Nondal, G., Slagstad, D., Czerny, J., de Lange, T., and Ludwig, A. 2012. Marine carbonate system evolution during the epoca arctic pelagic ecosystem experiment in the context of simulated arctic ocean acidification. Biogeosciences Discussions, 9: 15541–15565.

Blackford, J., and Gilbert, F. 2007. pH variability and CO_2 induced acidification in the North Sea. Journal of Marine Systems, 64: 229–241.

Bode, A., Barquero, S., Gonzales, N., Alvarez-Ossorio, M., and Varela, M. 2004. Contribution of heterotrophic plankton to nitrogen regeneration in the upwelling ecosystem of La Coruna (NW Spain). Journal of Plankton Research, 26: 11–28.

Børsheim, K., and Golmen, L. 2010. Forsuring av havet. Kunnskapsstatus for norske farvann. Tech. Rep. TA 2575/2010, KLIF, Oslo, Norway, 101 pp.

Broecker, W., and Peng, T-H. 1974. Gas exchange rates between air and sea. Tellus, 26: 21–35.

Caldeira, K., and Wickett, M. 2003. Anthropogenic carbon and ocean ph. Nature, 425: 365.

Chen, C., and Borges, A. 2009. Reconciling opposing views on carbon cycling in the coastal ocean: continental shelves as sinks and near-shore ecosystems as sources of atmospheric CO_2. Deep-Sea Research II, 56: 578–581.

Chierici, M., Skjelvan, I., Norli, M., Børsheim, K., Lauvset, S., Lødemel, H., Sørensen, K., *et al.* 2016. Overvåking av havforsuring i norske farvann i 2015. Tech. Rep. M-573, Miljødirektoratet, Oslo, Norway, 114 pp.

Dalpadado, P., Arrigo, A., Hjøllo, S., Rey, F., Ingvaldsen, R., Sperfeld, E., Dijken, G., *et al.* 2014. Productivity in the Barents Sea – response to recent climate variability. PLoS One, 9: e95273.

Dickson, A., and Millero, F. 1987. A comparison of the equilibrium constants for the dissociation of carbonic acid in seawater media. Deep-Sea Res, 34: 1733–1743.

ENSEMBLES, 2009. RCM-specific weights based on their ability to simulate the present climate calibrated for the ERA40-based simulations. ENSEMBLES (http://ensembles-eu.metoffice.com (last accessed 5 July 2018)) Project report D3.2.2 to the EU. 66pp. + 2app.

Eriksen, E., Ingvaldsen, R., Nedreaas, K., and Prozorkevich, D. 2015. The effect of recent warming on polar cod and beaked redfish juveniles in the Barents Sea. Regional Studies in Marine Science, 2: 105–112.

Feely, R., Doney, S., and Cooley, S. R. 2009. Ocean acidification: present conditions and future changes in a high-CO_2 world. Ocean Acidification. Present conditions and future changes in a high CO_2 world. Oceanography, 22: 36–47.

Fossheim, M., Primicerio, R., Johannesen, E., Ingvaldsen, R., Aschan, M., and Dolgov, A. 2015. Recent warming leads to a rapid borealization of fish communities in the Arctic. Nature Climate Change, 5: 673–678.

Garber, J. 1984. Laboratory study of nitrogen and phosphorous remineralization during decomposition of coastal plankton and seston. Estuarine, Coastal and Shelf Science, 18: 685–702.

Gehlen, M., Malschaert, H., and Raaphorst, W. 1995. Spatial and temporal variability of benthic silica fluxes in the southeastern North Sea. Continental Shelf Research, 15: 1675–1696.

Gent, P. R., Danabasoglu, G., Donner, L. J., Holland, M. M., Hunke, E. C., Jayne, S. R., Lawrence, D. M., *et al.* 2011. The community climate system model version 4. Journal of Climate, 24: 4973–4991.

Gharamti, M., Tjiputra, J., Bethke, I., Samuelsen, A., Skjelvan, I., Bentsen, M., and Bertino, L. 2017. Ensemble data assimilation for ocean biogeochemical state and parameter estimation at different sites. Ocean Modelling, 112: 65–89.

Hawkins, E., and Sutton, R. 2009. The potential to narrow uncertainty in regional climate predictions. Bulletin of the American Meteorological Society, 90: 1095–1107.

Hjøllo, S., Huse, G., Skogen, M. D., and Melle, W. 2012. Modelling secondary production in the Norwegian Sea with a fully coupled physical/primary production/individual-based *Calanus finmarchicus* model system. Marine Biology Research, 8: 508–526.

Ingri, N., Kakolowicz, W., Sillen, L., and Warnqvist, B. 1967. Highspeed computers as a supplement to graphical methods: v. HALTAFALL, a general program for calculating the composition of equilibrium mixtures. Talanta, 14: 1261.

IPCC, 2013. Annex II: climate system scenario tables. *In* Climate Change 2013: The Physical Science Basis. Contribution of Working Group I to the 5th Report of the Intergovernmental Panel on Climate Change, pp. 1395–1445. Ed. by Prather M., Flato G., Friedlingstein P., Jones C. and Lamarque J.. Cambridge University Press, Cambridge, United Kingdom/New York, NY, USA.

IPCC, 2014. Climate Change 2014: Synthesis Report. contribution of working groups i, ii and iii to the 5th assessment report of the Intergovernmental Panel on Climate Change. 151 pp.

Langehaug, H., Sandø, A., írthun, M., and Ilicak, M. 2018. Variability along the Atlantic water pathway in the forced Norwegian Earth System Model coastal zones. Climate Dynamics, 10.1007/s00382-018-4184-5.

Lauvset, S., Chierici, M., Counillon, F., Omar, A., Nondal, G., Johannessen, T., and Olsen, A. 2013. Annual and seasonal fCO_2 and air–sea CO_2 fluxes in the Barents Sea. Journal of Marine Systems, 113–114: 62–74.

Lauvset, S., Gruber, N., Landschutzer, P., Olsen, A., and Tjiputra, J. 2015. Trends and drivers in global surface ocean pH over the past 3 decades. Biogeosciences, 12: 1285–1298.

Lauvset, S. K., Key, R. M., Olsen, A., van Heuven, S., Velo, A., Lin, X., Schirnick, C., *et al.* 2016. A new global interior ocean mapped climatology: the 1×1 glodap version 2. Earth System Science Data, 8: 325–340.

Lohse, L., Kloosterhuis, H. T., van Raaphorst, W., and Helder, W. 1996. Denitrification rates as measured by the isotope pairing method and by the acetylene inhiluition technique in continental shelf sediments of the North Sea. Marine Ecology Progress Series, 132: 169–179.

Lohse, L., Malschaert, F., Slomp, C., Helder, W., and Raaphorst, W. 1995. Sediment-water fluxes of inorganic nitrogen compounds along the transport route of organic matter in the North Sea. Ophelia, 41: 173–197.

Lønborg, C., Davidson, K., Alvarez-Salgado, X., and Miller, A. 2009. Bioavailability and bacterial degradation rates of dissolved organic matter in a temperate coastal area during an annual cycle. Marine Chemistry, 113: 219–226.

Maier-Reimer, E., Kriest, I., Segschneider, J., and Wetzel, P. 2005. The Hamburg Oceanic Carbon Cycle Circulation Model hamocc5.1 – Technical Description Release 1.1. Tech. Rep. Reports on Earth System Science 14, Max Planck Institute for Meteorology, Hamburg, Germany.

Manizza, M., Follows, M., Dutkiewicz, S., Menemenlis, D., Hill, C., and Key, R. 2013. Changes in the Arctic Ocean CO_2 sink (1996–2007): a regional model analysis. Global Biogeochemical Cycles, 27: 1108–1118.

Martinsen, E., and Engedahl, H. 1987. Implementation and testing of a lateral boundary scheme as an open boundary condition in a barotropic ocean model. Coastal Engineering, 11: 603–627.

Matear, R., and Hirst, A. 1999. Climate change feedback on the future oceanic CO_2 uptake. Tellus B: Chemical and Physical Meteorology, 51: 722–733.

Mayer, B. 1995. Ein dreidimensionales, numerisches schwebstoff-transportmodell mit anwendung auf die Deutsche Bucht. Tech. Rep. GKSS 95/E/59, GKSS-Forschungszentrum Geesthacht GmbH, ISSN:0344-9629, 104 pp.

Mehrbach, C., Culberson, C. H., Hawley, J. E., and Pytkowicx, R. M. 1973. Measurement of the apparent dissociation constants of carbonic acid in seawater at atmospheric pressure. Limnology and Oceanography, 18: 897–907.

Melsom, A., Lien, V., and Budgell, W. 2009. Using the regional ocean modeling system (ROMS) to improve the ocean circulation from a GCM 20th century simulation. Ocean Dynamics, 59: 969–981.

Moll, A., and Stegert, C. 2007. Modeling pseudocalanus elongatus population dynamics embedded in a water column ecosystem model for the northern North Sea. Journal of Marine Systems, 64: 35–46.

Nightingale, P., Malin, G., Law, C., Watson, A., Liss, P., Liddicoat, M., Boutin, J., *et al.* 2000. In situ evaluation of air–sea gas exchange parameterizations using novel conservative and volatile tracers. Global Biogeochemical Cycles, 14: 373–388.

Olafsson, J., Olafsdottir, S., Benoit-Cattin, A., Danielsen, M., Arnarson, T., and Takahashi, T. 2009. Rate of Iceland Sea acidification from time series measurements. Biogeosciences, 6: 2661–2668.

Olsen, A., Key, R., van Heuven, S., Lauvset, S., Velo, A., Lin, X., Schirnick, C., *et al.* 2016. The global ocean data analysis project version 2 (GLODAPv2) – an internally consistent data product for the world ocean. Earth System Science Data, 8: 297–323.

Olsen, A., Omar, A., Bellerby, R., Johannessen, T., Ninnemann, U., Brown, K., Olsson, K., *et al.* 2006. Magnitude and origin of the anthropogenic CO_2 increase and ^{13}C suess effect in the Nordic seas since 1981. Global Biogeochemical Cycles, 20: GB3027, doi: 10.1029/2005GB002669.

Orr, J., Fabry, V., Aumont, O., Bopp, L., Doney, S., Feely, R. A. G., Gruber, N., *et al.* 2005. Anthropogenic ocean acidification over the twenty-first century and its impact on calcifying organisms. Nature, 437: 681–686.

Overland, J., and Wang, M. 2007. Future regional Arctic sea ice declines. Geophysical Research Letters, 34: L17705.

Pätsch, J., Kühn, W., and Moll, A. H. L. 2009. ECOHAM4 user guide – ECOsystem model, HAMburg, version 4. Tech. Rep. 01-2009, Institut Für Meereskunde, Hamburg, Germany.

Pohlmann, T., and Puls, W. 1994. Currents and transport in water, *In* Circulation and Contaminant Fluxes in the North Sea, pp. 345–402. Ed. by J. Sündermann. Springer Verlag, Berlin.

Rey, F. 2004. Phytoplankton: the grass of the sea. *In* The Norwegian Sea Ecosystem, pp. 97–136. Ed. by H. Skjoldal. Tapir Academic Press, Trondheim, Norway.

Rey, F., Noji, T., and Miller, L. 2000. Seasonal phytoplankton development and new production in the Central Greenland Sea. Sarsia, 85: 329–344.

Richardson, K., Markager, S., Buch, E., Lassen, M., and Kristensen, A. 2005. Seasonal distribution of primary production, phytoplankton biomass and size distribution in the Greenland Sea. Deep-Sea Research I, 52: 979–999.

Roleda, M., Boyd, P., and Hurd, C. 2012. Before ocean acidification: calcifier chemistry lessons. Journal of Phycology, 48: 840–843.

Saini, R., Wang, G., Yu, M., and Kim, J. 2015. Comparison of RCM and GCM projections of boreal summer precipitation over Africa. Journal of Geophysical Research: Atmospheres, 120: 3679–3699.

Sandø, A., Melsom, A., and Budgell, P. 2014. Downscaling IPCC control run and future scenario with focus on the Barents Sea. Ocean Dynamics, 64: 927–949.

Sandø, A., Mousing, E., Budgell, W., Hjøllo, S., Skogen, M., and ídlandsvik, B. 2018. Possible Barents Sea climate and ecosystem changes in a moderate future emission scenario (RCP4.5). Manuscript in Preparation.

Shchepetkin, A. F., and McWilliams, J. C. 2005. The regional oceanic modeling system (ROMS): a split-explicit, free-surface, topography-following-coordinate oceanic model. Ocean Modelling, 9: 347–404.

Six, K. D., and Maier-Reimer, E. 1996. Effects of plankton dynamics on seasonal carbon fluxes in an ocean general circulation model. Global Biogeochemical Cycle, 10: 559–583.

Skaret, G., Dalpadado, P., Hjøllo, S., Skogen, M., and Strand, E. 2014. *Calanus finmarchicus* abundance, production and population dynamics in the Barents Sea in a future climate. Progress in Oceanography, 125: 26–39.

Skartveit, A., and Olseth, J. A. 1986. Modelling slope irradiance at high lattitudes. Solar Energy, 36: 333–344.

Skartveit, A., and Olseth, J. A. 1987. A model for the diffuse fraction of hourly global radiation. Solar Energy, 38: 271–274.

Skjelvan, I., Falck, E., Rey, F., and Kringstad, S. 2008. Inorganic carbon time series at Ocean Weather Station M in the Norwegian Sea. Biogeosciences, 5: 549–560.

Skogen, M., Budgell, W., and Rey, F. 2007. Interannual variability in Nordic Seas primary production. ICES Journal of Marine Science, 64: 889–898.

Skogen, M., and Moll, A. 2000. Interannual variability of the North Sea primary production: comparison from two model studies. Continental Shelf Research, 20: 129–151.

Skogen, M., and Moll, A. 2005. Importance of ocean circulation in ecological modelling: an example from the North Sea. Journal of Marine Systems, 57: 289–300.

Skogen, M., Olsen, A., Børsheim, K., Sandø, A., and Skjelvan, I. 2014. Modelling ocean acidification in the Nordic and Barents seas in present and future climate. Journal of Marine Systems, 131: 10–20.

Skogen, M., and Søiland, H. 1998. A user's guide to NORWECOM v2.0. The NORWegian ECOlogical Model system. Tech. Rep. Fisken Og Havet 18/98, Institute of Marine Research, Pb.1870, NO-5024 Bergen, 42 pp.

Skogen, M., Svendsen, E., Berntsen, J., Aksnes, D., and Ulvestad, K. 1995. Modelling the primary production in the North Sea using a coupled 3 dimensional Physical Chemical Biological Ocean model. Estuarine, Coastal and Shelf Science, 41: 545–565.

Slagstad, D., Ellingsen, I., and Wassmann, P. 2011. Evaluating primary and secondary production in an Arctic Ocean void of summer sea ice: an experimental simulation approach. Progress in Oceanography, 90: 117–131. arctic Marine Ecosystems in an Era of Rapid Climate Change. http://www.sciencedirect.com/science/article/pii/S0079661111000243 (last accessed 5 July 2018).

Slagstad, D., Wassmann, P., and Ellingsen, I. 2015. Physical constrains and productivity in the future Arctic Ocean. Frontiers in Marine Science, 2: 85.

Stegert, C., Moll, A., and Kreus, M. 2009. Validation of the three-dimensional ECOHAM model in the German Bight for 2004 including population dynamics of pseudocalnus elongatus. Journal of Sea Research, 62: 1–15.

Steinacher, M., Joos, F., Frölicher, T., Bopp, L., Cadule, P., Cocco, V., Doney, S., *et al.* 2010. Projected 21st century decrease in marine productivity: a multi-model analysis. Biogeosciences, 7: 979–1005.

Steinacher, M., Joos, F., Frölicher, T., Plattner, G-K., and Doney, S. 2009. Imminent ocean acidification in the Arctic projected with NCAR global coupled carbon cycle climate model. Biogeosciences, 6: 515–533.

Taylor, J. R., and Ferrari, R. 2011. Shutdown of turbulent convection as a new criterion for the onset of spring phytoplankton blooms. Limnology and Oceanography, 56: 2293–2307.

Taylor, K. E., Stouffer, R. J., and Meehl, G. A. 2012. An overview of CMIP5 and the experiment design. Bulletin of the American Meteorological Society, 93: 485–498.

Titov, O. 1995. Seasonal dynamics of primary produciton in the Barents sea. ICES CM 1995/Mini: 16. Mini-Symposium on Arctic Oceanographic Processes. ICES (International Council for the Exploration of the Seas, Copenhagen, Denmark).

Titov, O., and Orlova, E. 2011. Lower trophic levels. *In* The Barents Sea. Ecosystem, Resources and Management. Half a Century of Russian-Norwegian Cooperation, pp. 77–119. Ed. by T. Jakobsen and V. Ozhigin. Tapir Academic Press, Trondheim, Norway, 825 pp.

Tjiputra, J., Polzin, D., and Winguth, A. 2007. Assimilation of seasonal chlorophyll and nutrient data into an adjoint threedimensional ocean carbon cycle model: sensitivity analysis and ecosystem parameter optimization. Global Biogeochemical Cycles, 21: 10.1029/2006GB002745.

Tjiputra, J. F., Roelandt, C., Bentsen, M., Lawrence, D. M., Lorentzen, T., Schwinger, J., Seland, Ø., *et al.* 2013. Evaluation of the carbon cycle components in the Norwegian Earth System Model (NorESM). Geoscientific Model Development, 6: 301–325.

Troupin, C., Barth, A., Sirjacobs, D., Ouberdous, M., Brankart, J-M., Brasseur, P., Rixen, M., *et al.* 2012. Generation of analysis and consistent error fields using the data interpolating variational analysis (diva). Ocean Modelling, 52–53: 90–101.

Utne, K., Hjøllo, S., Huse, G., and Skogen, M. 2012. Estimating consumption of *Calanus finmarchicus* by planktivorous fish in the norwegian sea using a fully coupled 3d model system. Marine Biology Research, 8: 527–547.

Yasunaka, S., Murata, A., Watanabe, E., Chierici, M., Fransson, A., van Heuven, S., Hoppema, M., *et al.* 2016. Mapping of the airesea CO_2 flux in the Arctic Ocean and its adjacent seas: basin-wide distribution and seasonal to interannual variability. Polar Science, 10: 323–334.

Handling editor: Morgane Travers-Trolet